Available online at ScienceDirect

Nuclear Engineering and Technology

journal homepage: www.elsevier.com/locate/net

Original Article

Study on the Structure Optimization and the Operation Scheme Design of a Double-Tube Once-Through Steam Generator

CrossMark

Xinyu Wei[*], *Shifa Wu, Pengfei Wang, and Fuyu Zhao*

Department of Nuclear Science and Technology, Xi'an Jiaotong University, Xi'an, Shaanxi 710049, China

A B S T R A C T

A double-tube once-through steam generator (DOTSG) consisting of an outer straight tube and an inner helical tube is studied in this work. First, the structure of the DOTSG is optimized by considering two different objective functions. The tube length and the total pressure drop are considered as the first and second objective functions, respectively. Because the DOTSG is divided into the subcooled, boiling, and superheated sections according to the different secondary fluid states, the pitches in the three sections are defined as the optimization variables. A multi-objective optimization model is established and solved by particle swarm optimization. The optimization pitch is small in the subcooled region and superheated region, and large in the boiling region. Considering the availability of the optimum structure at power levels below 100% full power, we propose a new operating scheme that can fix the boundaries between the three heat-transfer sections. The operation scheme is proposed on the basis of data for full power, and the operation parameters are calculated at low power level. The primary inlet and outlet temperatures, as well as flow rate and secondary outlet temperature are changed according to the operation procedure.

1.   Introduction

In a nuclear power plant (NPP), the steam generator (SG) is an important piece of equipment that exchanges heat from the reactor core to the secondary loop and supplies steam to the turbine, generating electricity or providing power. In many integrated nuclear power plants (iNPPs) such as mPower, NuScle, and WSMR, a once-through steam generator (OTSG) is always used because it can enhance the heat-transfer capacity and can decrease the volume and weight of the entire iNPP [1,2].

The OTSG has no steam drum because 100% of the flowing water evaporates within the heat-transfer tubes. There are two main types of tubes in an OTSG: the helical coil tube and
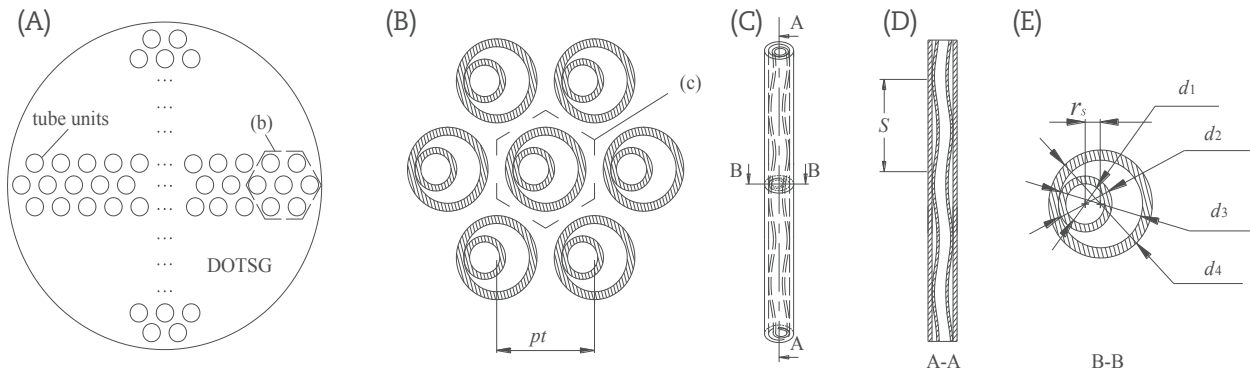
Fig. 1 – Structure of the DOTSG. (A) Cross-section of the DOTSG; (B) its partial details; (C) perspective view of a single tube unit; (D) vertical section of A–A in (C); and (E) cross-section of B–B in (C). d_1, inner diameter of the inner tube; d_2, outer diameter of the inner tube; d_3, inner diameter of the outer tube; d_4, outer diameter of the outer tube; DOTSG, double-tube once-through steam generator; pt, central axis distance of the outer tubes; r_S, helical radius of the inner helical tube; S, the pitch of the inner helical tube.

the straight tube. The helical coil tube can reduce stress caused by thermal expansion and can increase the heat-transfer area. The straight tube reduces the secondary pressure drop and has a simple structure, which is beneficial to the manufacture and maintenance of the OTSG. To combine the advantages of the two tube types, a double-tube once-through steam generator (DOTSG) having a tube unit consisting of an outer straight tube and an inner helical tube is presented in this paper. Fig. 1 illustrates the structure of the DOTSG.

Fig. 2 is a schematic diagram of the operation of an iNPP with the DOTSG. The primary water coming from the reactor core enters from the top of the DOTSG. The water then travels downward through the tubes, finally exiting at the bottom of the DOTSG and returning to the reactor vessel. Flow passages in the reactor vessel constitute the primary loop; this part is defined as the primary side of the SG. As the primary water travels down the metal tubes, the water transfers heat to the secondary fluid. The secondary water coming from the feedwater supply system is pumped into the bottom of the DOTSG. The temperature rises when the water flows upward. The boiling process continues until the steam reaches a quality of one. The saturation steam becomes superheated and then
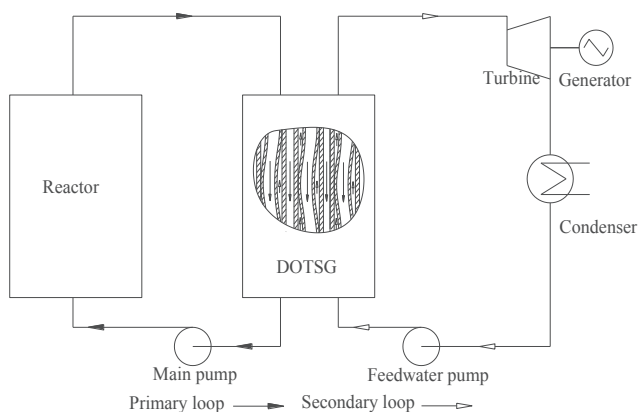
leaves the DOTSG through the steam valve. Flow passage through the turbine, condenser, and feedwater pump comprises the secondary loop; this part of the DOTSG is defined as the secondary side.

On the primary side, water flows through the inner helical tube and shell side; while on the secondary side, the fluid flows through the lunate channel between the outer straight tube and the inner helical tube. On both sides of the inner helical tube, the spiral flow enhances heat transfer but the flow resistance increases, strongly influencing the main pump and feedwater pump.

According the descriptions above, the DOTSG is a type of bilaterally heated narrow-annuli heat exchanger. Many studies have been performed on the heat-exchange problem in bilaterally heated narrow annuli and helical tubes. However, the optimization problem is rarely addressed in these studies. Roy et al. [3,4] used both experimental methods and simulation to study the isothermal and heated turbulent upflow in a vertical annular channel. They observed buoyancy effects on the velocity and thermal fields in the simulation results and in the measurements. In an experimental investigation on the flow and heat transfer in narrow annuli, Wang et al. [5] showed that when the heat flux values of both sides of the narrow annuli are equal, the heat-transfer coefficient of the inner tube is greater than that of the outer tube, and the heat-transfer rate of the annuli is the highest. Chen et al. [6] used the smallest difference in the outlet temperatures of the two primary sides to optimize the flow distribution. To reach the optimized flow distribution, the gap width was varied according to the tube dimensions. Results of an immovable enthalpy boundary model developed by Yu and Jia [7] for the heat-transfer calculation of a DOTSG with an inner helical tube indicate that the inner helical tube enhances the heat transfer. However, the pressure drop was not considered in their study. Some investigators have considered that the minimum cost of the heat-transfer surface area or capital investment to be an objective function to optimize the heat exchanger [8,9]. Others have considered the sum of investment related to the heat-transfer surface area and operational costs (fluid head losses) as an objective function for the
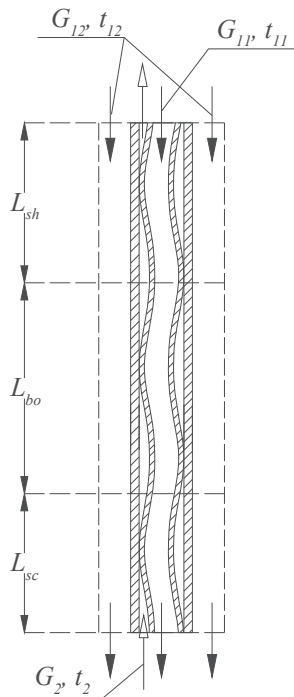

Fig. 2 – Schematic diagram for the operation of an integrated nuclear power plant with the double-tube once-through steam generator (DOTSG).

Fig. 3 − The three streams of the double-tube once-through steam generator (DOTSG) and the division of the heat-transfer section. L_{sc}, L_{bo}, and L_{sh} are the lengths of the subcooled, boiling, and superheated sections, respectively; G_2, G_{11}, and G_{12} are the mass flow rates of the secondary side, primary side in the inner tube, and primary side in the shell side, respectively; and t_2, t_{11}, and t_{12} are the temperatures of the secondary side, primary side in the inner tube, and primary side in the shell side, respectively.

optimization [10,11]. Johannessen et al. [12] used the sum of the entropy generation of the streams as an objective function in their optimization study. The particle swarm optimization (PSO) method, a type of artificial intelligence algorithm, finds a global optimum more easily by using iterative searching methods. Being a derivative-free and population-based stochastic search algorithm, PSO is robust and fast in solving nonlinear, multi-objective problems. Moreover, PSO is easy to implement and allows a straightforward understanding of the searching trajectories [13]. It has been widely used in nuclear engineering, such as in the optimization of the energy group structure [14], optimization of a U-tube SG [15], and visualization of two-phase flows [16].

We have completed some work on the structure optimization of the DOTSG using the non-dominated sorting genetic algorithm II and Pontryagin's maximum principle [17,18]. The optimized pitches of the inner helical tube in three heat-transfer regions have been determined. However, new problems arose during our study. Our previous optimization works were based on the stability state of 100% full power (FP); during the power change operation of the DOTSG, however, the boundaries of the heat-transfer regions change, this necessitating analysis of the optimum structure of the DOTSG during the power change operation. This paper shows two main contributions to our work. One is the optimization of the

DOTSG by PSO, and the other is the design of a new operation scheme for the optimum DOTSG that fits its fixed optimization structure.

This paper is structured as follows. In Section 2, we introduce the heat-transfer process and the pressure drop calculation for the DOTSG. For the DOTSG's structure operation, we establish and solve a multi-objective problem by PSO in Section 3. In Section 4, the power change operation of the DOTSG is analyzed and a new operation scheme is designed. Finally, we conclude in Section 5.

2.   Formula description

Assuming that every tube unit of the DOTSG has an identical flow, we may analyze the SG by using the single module concept, that is, the SG is treated as a single-module heat exchanger. This type of heat transfer is divided into three sections according to the secondary water/steam status (Fig. 3), namely, the subcooled, boiling, and superheated sections. In the subcooled and superheated sections, the secondary fluids are subcooled water and superheated steam, respectively, both of which are single phases. In the boiling section, the secondary fluid is a mixture of steam and water (two-phase). In every tube unit of the DOTSG, the primary water flows in the inner helical tube and the shell side, while the secondary fluid flows in the channel consisting of the outer straight tube and the inner helical tube. Fig. 3 shows the three streams in a single tube unit of the DOTSG and the division of the heat-transfer section.

To compact the SG and to reduce the pressure drop, we considered the reduction of tube length and the pressure drop as two objective functions under a constant heat duty. Thus, the heat-transfer process and pressure drop calculation are discussed in this section.

2.1.   Heat-transfer calculation

In the DOTSG, the secondary fluid obtains heat from the primary water in the inner helical tube and shell side. The basic equation of the heat transfer based on the energy conservation principle can be expressed as Eq. (1).

$$Q = U_{11}A_{11}LMTD_{11} + U_{12}A_{12}LMTD_{12} \qquad (1)$$

where Q is the heat transfer rate, U_{11} is the overall heat-transfer coefficient based on the outer area of the inner helical tube, U_{12} is the overall heat-transfer coefficient based on the inner area of the outer tube, A_{11} is the heat-transfer surface area of the outer surface of the inner helical tube, A_{12} is the heat-transfer surface area of the inner surface of the outer tube, $LMTD_{11}$ is the log-mean temperature difference of the primary water in the inner helical tube and the secondary fluid, and $LMTD_{12}$ is the log-mean temperature difference of the primary water in shell side and the secondary fluid. A_{11}, A_{12} are computed through Eqs. (2−4).

$$A_{11} = \pi d_2 L_s \qquad (2)$$

$$A_{12} = \pi d_3 \tag{3}$$

$$L_s/L = \left[\sqrt{S^2 + (\pi d_3)^2} \right] \Big/ S \tag{4}$$

where d_2 is the outer diameter of the inner helical tube, d_3 is the inner diameter of the outer tube, L is the length of the straight tube, L_s is the length of the inner helical tube, and S is the pitch of the inner helical tube, which corresponds to the axial length of one coil of the helical tube. Inputting Eqs. (2−4) into Eq. (1) and subsequent rearrangements give the first objective function:

$$L = Q \left/ \left\{ U_{11} \pi d_2 LMTD_{11} \frac{\sqrt{S^2 + (\pi d_3)^2}}{S} + U_{12} \pi d_3 LMTD_{12} \right\} \right. \tag{5}$$

The overall heat-transfer coefficients in Eq. (1) are computed in Eqs. (6) and (7).

$$U_{11} = 1 \left/ \left(\frac{d_2}{\alpha_{11} d_1} + \frac{d_2}{2\lambda_{itube}} \ln \frac{d_2}{d_1} + \frac{1}{\alpha_2} \right) \right. \tag{6}$$

$$Nu_2 = \begin{cases} 0.002 \left[1 + 68.2 \left(\frac{S}{d_3} \right)^{-0.21} \right] \left(\frac{d_2}{d_3} \right)^{-0.4} Re_2^{\left\{ 0.002 \left[1 + 68.2 \left(\frac{S}{d_3} \right)^{0.73} \right] \right\}} Pr_2^{0.43} \left(\frac{Pr_2}{Pr_w} \right)^{0.25}, & 2 \times 10^3 \le Re_2 \le Re_{2,cr},\ 0.040 \le S \le 0.064 \\[2ex] 0.002 \left[1 + 1.25 \times 10^6 \left(\frac{S}{d_3} \right)^{-6.37} \right] \left(\frac{d_2}{d_3} \right)^{-0.4} Re_2^{\left\{ 0.6 \left[1 + 0.0165 \left(\frac{S}{d_3} \right)^{1.68} \right] \right\}} Pr_2^{0.43} \left(\frac{Pr_2}{Pr_w} \right)^{0.25}, & 2 \times 10^3 \le Re_2 \le Re_{2,cr},\ 0.064 \le S \le 0.120 \\[2ex] 0.015 \left[1 + 5.39 \left(\frac{S}{d_3} \right)^{-0.9} \right] \left(\frac{d_2}{d_3} \right)^{-0.35} Re_2^{0.8} Pr_2^{0.43} \left(\frac{Pr_2}{Pr_w} \right)^{0.25}, & Re_{2,cr} \le Re_2 \le 4 \times 10^4,\ 0.040 \le S \le 0.064 \\[2ex] 0.015 \left[1 + 182 \left(\frac{S}{d_3} \right)^{-3.04} \right] \left(\frac{d_2}{d_3} \right)^{-0.35} Re_2^{0.8} Pr_2^{0.43} \left(\frac{Pr_2}{Pr_w} \right)^{0.25}, & Re_{2,cr} \le Re_2 \le 4 \times 10^4,\ 0.064 \le S \le 0.120 \end{cases} \tag{10}$$

$$U_{12} = 1 \left/ \left(\frac{d_3}{\alpha_{12} d_4} + \frac{d_3}{2\lambda_{otube}} \ln \frac{d_4}{d_3} + \frac{1}{\alpha_2} \right) \right. \tag{7}$$

where α_{11} is the convective-heat-transfer coefficient of the primary water in the inner helical tube, α_{12} is the convective-heat-transfer coefficient of the primary water in the shell side, α_2 is the convective-heat-transfer coefficient of the secondary fluid, λ_{itube} is the thermal conductivity of the inner helical tube, λ_{otube} is the thermal conductivity of the outer tube, d_1 is the inner diameter of the inner helical tube, and d_4 is the outer diameter of the outer tube. α_{11} and α_{12} are, respectively, obtained by using the Dittus−Boelter equation and a modification of the equation [Eq. (8)] [18].

$$\alpha_{11} = 1.3 \times 0.023 \frac{\lambda_{11}}{d_1} Re_{11}^{0.8} Pr_{11}^{0.3} \tag{8}$$

where λ_{11} is the thermal conductivity of the primary water in the inner helical tube, Re_{11} is the Reynolds number of the primary water in the inner helical tube, and Pr_{11} is the Prandtl number of the primary water in the inner helical tube.

The convective-heat-transfer coefficient of the secondary fluid based on the pitch is obtained from the experimental results [19] under the following conditions: non-adiabatic flow, $P = 3.0 - 6.5\,MPa$, $\rho v = 50 - 450\,kg/m^2 s$, and $q = 0.04 - 0.25\,MW/m^2$. The results show that the convective-heat-transfer coefficient of the secondary fluid varied in the different heat-transfer sections. In the subcooled section and superheated sections, the convective-heat-transfer coefficients of the secondary side are calculated through Eq. (9).

$$\alpha_2 = \frac{\lambda_2}{d_{e,2}} Nu_2 \tag{9}$$

where λ_2 is the thermal conductivity of the secondary fluid, $d_{e,2}$ is the hydraulic diameter of the secondary channel, and Nu_2 is the Nusselt number of the secondary fluid, which is calculated through Eq. (10).

where Re_2 is the Reynolds number of the secondary fluid, Pr_2 is the Prandtl number of the secondary fluid, and Pr_w is the Prandtl number of the secondary fluid at the temperature of the wall. $Re_{2,cr}$ is the critical Reynolds number, which de-

scribes the transition of laminar flow to turbulent flow. It is computed through Eq. (11).

$$Re_{2,cr} = 18500 \left[\frac{d_3 - d_2}{\sqrt{S^2/4 + (d_3 - d_2)^2}} \right]^{0.3} \tag{11}$$

In the boiling section, the convective-heat-transfer coefficients of the secondary side are calculated through Eq. (12).

$$\alpha_2 = \alpha_L \sqrt{1 + 0.6(\alpha_0/\alpha_L)^2} \tag{12}$$

where α_L is the convective-heat-transfer coefficient of the saturated water calculated from Eq. (10), and α_0 is the convective-heat-transfer coefficient when the inner tube is straight, as calculated from Eq. (13).

$$\alpha_0 = 4.6 q^{0.7} p^{0.2} \tag{13}$$

where q is the heat flux and p is the pressure.

As we could not know the heat flux without the convective-heat-transfer coefficient, we computed the tube length of the boiling section iteratively as follows:

Step 1: Give the initial value of the heat flux q.

Step 2: Calculate the length of the boiling section L_{bo} and of the heat-transfer surface areas A_{11}, A_{12} using Eqs. (5), (2), and (3), respectively.

Step 3: Calculate the iterative heat flux q' using Eq. (14).

$$q' = \frac{Q}{A_{11} + A_{12}} \tag{14}$$

Step 4: Compare q and q' using Eq. (15). If it is true, then go to Step 5; otherwise, let $q = q'$ and return to Step 2.

$$|q - q'| \leq \varepsilon \tag{15}$$

Step 5: Save and finish.

2.2. *Pressure drop calculation*

The pressure drops in the three flow passages of the DOTSG are calculated individually. The pressure drop in each passage contains the frictional pressure drop, acceleration pressure drop, and gravitational pressure drop. Because the pitch mainly affects the frictional pressure drop but not the acceleration and gravitational pressure drops, we consider only the frictional pressure drop in this paper.

The frictional pressure drop in the helical tube may be calculated through Eq. (16).

$$\Delta p_{11} = f_{11} \frac{\rho_{11} v_{11}^2}{2d_1} L \tag{16}$$

where f_{11} is the friction factor of the primary side in the inner tube, ρ_{11} is the density of the primary water in the inner tube, and v_{11} is the average velocity of the primary water in the inner tube. ρ_{11} and v_{11} may be obtained through the results of the heat-transfer calculation. The friction factor, f_{11}, may be calculated through Eq. (17) [20].

$$f_{11} = \begin{cases} 3.5\left[1 + 30\left(\frac{S}{r_s}\right)^{-1.3}\right]\left(1 + \frac{r_s}{d_2}\right)^{0.54} Re_{11}^{-0.55}, \\ \quad 2 \times 10^3 \leq Re_{11} \leq Re_{11,cr} \\ 0.316\left[1 + 1.2 \times 10^3\left(\frac{S}{r_s}\right)^{-3}\right]\left(1 + \frac{r_s}{d_2}\right)^{0.46} Re_{11}^{-0.25}, \\ \quad Re_{11,cr} \leq Re_{11} \leq 8 \times 10^4 \end{cases} \tag{17}$$

where r_s is the helical radius of the inner helical tube, and $Re_{11,cr}$ is the critical Reynolds number of the helical tube, which is computed from Eq. (18).

$$Re_{11,cr} = 22000\left(\frac{S}{r_s}\right)^{-0.3} \tag{18}$$

The frictional pressure drop of the shell side is calculated through Eq. (19).

$$\Delta p_{12} = f_{12} \frac{\rho_{12} v_{12}^2}{2d_{e,12}} L \tag{19}$$

where f_{12} is the friction factor of the primary side of the shell side, ρ_{12} is the density of the primary water in the shell side, and v_{12} is the average velocity of the primary water in the shell side. ρ_{12} and v_{12} may be obtained by calculating the heat transfer. The friction factor f_{12} is computed by using the Sieder−Tate formula.

The pressure drop in the secondary side based on the pitch is obtained from experimental results [20] under the following conditions: non-adiabatic flow, $P = 3.0 - 6.5$ MPa, $\rho v = 50 - 450$ kg/m^{2}s, and $q = 0.04 - 0.25$ MW/m^2. In the subcooled and superheated sections,

$$\Delta p_2 = f_2 \frac{\rho_2 v_2^2}{2d_{e,2}} L \tag{20}$$

where f_2 is the friction factor of the secondary side, ρ_2 is the density of the secondary side, and v_2 is the average velocity of the secondary side. The friction factor may be calculated from Eq. (21).

$$f_2 = \begin{cases} 0.5\left[1 + 28\left(\frac{S}{d_3}\right)^{-1.6}\right]\left(\frac{d_2}{d_3}\right)^{-0.64} Re_2^{\left\{-0.25\left[1+0.92\left(\frac{S}{d_3}\right)^{-0.3}\right]\right\}}, \\ \quad 2 \times 10^3 \leq Re_2 \leq Re_{2,cr}, \; 0.040 \leq S \leq 0.064 \\ 0.5\left[1 + 706\left(\frac{S}{d_3}\right)^{-3.6}\right]\left(\frac{d_2}{d_3}\right)^{-0.64} Re_2^{\left\{-0.25\left[1+4.5\left(\frac{S}{d_3}\right)^{-1.2}\right]\right\}}, \\ \quad 2 \times 10^3 \leq Re_2 \leq Re_{2,cr}, \; 0.064 \leq S \leq 0.120 \\ 0.316\left[1 + 10\left(\frac{S}{d_3}\right)^{-2}\right]\left(\frac{d_2}{d_3}\right)^{-0.46} Re_2^{-0.25} \\ \quad Re_{2,cr} \leq Re_2 \leq 4 \times 10^4, \; 0.040 \leq S \leq 0.064 \\ 0.316\left[1 + 12.6\left(\frac{S}{d_3}\right)^{-2.1}\right]\left(\frac{d_2}{d_3}\right)^{-0.46} Re_2^{-0.25}, \\ \quad Re_{2,cr} \leq Re_2 \leq 4 \times 10^4, \; 0.064 \leq S \leq 0.120 \end{cases} \tag{21}$$

In the boiling section, the frictional pressure drop is obtained from Eq. (22).

$$\Delta p_2 = \Psi\left[1 + x\left(\frac{\rho_L}{\rho_G} - 1\right)\right]\Delta p_0 \tag{22}$$

where Δp_0 is the single-phase frictional pressure drop of saturated water at the temperature of the boiling section, which may be calculated according to Eq. (21). ρ_L and ρ_G are, respectively, the densities of saturated water and saturated steam at the temperature of the boiling section. x is the quality of the secondary fluid, which is a mixture of water and steam; and Ψ is the non-uniform coefficient, which is calculated through Eq. (23).

$$\Psi = A_0 + \sum_{n=1}^{4} A_n x^n \tag{23}$$

where $A_n (n = 0,1,2,3,4)$ are constants when $P = 4$ MPa, $A_0 = 1$, $A_1 = 2.28$, $A_2 = -5.91$, $A_3 = 7.94$, and $A_4 = -3.94$; and when $P = 6$ MPa, $A_0 = 1.32$, $A_1 = -5.3$, $A_2 = 24.1$, $A_3 = -35.1$, and $A_4 = 16.8$.

R is defined as the flow resistance in a flow passage:

$$R = \frac{\Delta p}{V} \tag{24}$$

where V is the volume flow rate, which may be calculated from Eq. (25),

$$V = \frac{G}{\rho} \tag{25}$$

where G is the mass flow rate. e is defined as the ratio of the mass flow rate of the primary side in the inner helical tube to that of the primary side.

$$e = \frac{G_{11}}{G_1} \tag{26}$$

where G_{11} is the mass flow rate of the primary side in the inner helical tube, and G_1 is the total mass flow rate of the primary side.

Both of the primary side passages are parallel pipelines. They have the same pressure drop at the end of each branch. Thus, the pressure drop of the primary side should be calculated iteratively as follows:

Step 1: Give the initial value of e.

Step 2: Calculate the pressure drop of Δp_{11} and Δp_{12} using Eqs. (16) and (19), respectively.

Step 3: Compare Δp_{11} and Δp_{12} in Eq. (27). If Eq. (27) is true, then go to Step 4; otherwise, let $e = e^{'}$. and return to Step 2.

$$|\Delta p_{11} - \Delta p_{12}| \leq \varepsilon \tag{27}$$

Step 4: Let $\Delta p_1 = \Delta p_{11}$, and save it.

An expression for the new e in the iteration based on the average temperature of the two primary sides may be obtained from Eq. (28) by combining Eqs. (24−26).

$$e = \frac{\Delta p_{11}/R_{11}}{\Delta p_{11}/R_{11} + \Delta p_{12}/R_{12}} \tag{28}$$

The combined pressure drop, e, which is the second objective function of this work, may then calculated iteratively from Eq. (29).

$$\Delta p = \Delta p_1 + \Delta p_2 \tag{29}$$

3. Structure optimization of the DOTSG by PSO

3.1. PSO

The PSO method is one of the evolutionary techniques—its creation was inspired by swarms, such as those of insects, fish, or birds, and their coordinated movements [13]. In PSO, each of the particles or swarms is described by its position, and a velocity vector flies through the search space by following the current optimum particle. Particle motions are defined by a vector that defines the velocity of the swarm along each axis. The best solution for each particle obtained is stored in the particle memory and is named the particle experience. We use a separate memory (indicated as *pbest*) in which each particle stores the best position it has ever visited in the search space; the overall best position for all of the particles is indicated as *gbest*. During tracking of *pbest* and *gbest*, separate random numbers are generated for acceleration toward the two best positions. In this way, each particle of the swarm decides on its next movement

according to its own experience and the experience of the entire group.

Let Φ be an n-dimensional search space, f_{obj} be the objective function, and m be the number of particles that comprise the swarm, $\Phi = \{\vec{x}_1, \vec{x}_2, ..., \vec{x}_m\}$. The ith particle is a point in the search space with position $\vec{x}_i = \{x_{i,1}, x_{i,2}, ..., x_{i,n}\}$, velocity $\vec{v}_i = \{v_{i,1}, v_{i,2}, ..., v_{i,n}\}$, and individual best position $\vec{p}_i = \{p_{i,1}, p_{i,2}, ..., p_{i,n}\}$. $\vec{p}_i$ stores the best position ever visited by the ith particle during the search. The best position for all of the particles in the swarm is represented by $\vec{p}_g = \{p_{g,1}, p_{g,2}, ..., p_{g,n}\}$. The modified velocity and position of each particle may be calculated by using the current velocity and the distance from $\vec{p}_i$ to $\vec{p}_g$ as shown in Eqs. (30) and (31) [21].

$$v_{i,j}(t+1) = wv_{i,j}(t) + c_1 r_1 \left[p_{i,j}(t) - x_{i,j}(t) \right] + c_2 r_2 \left[p_{g,j}(t) - x_{i,j}(t) \right] \tag{30}$$

$$x_{i,j}(t+1) = x_{i,j}(t) + v_{i,j}(t+1) \tag{31}$$

where $i = 1, 2,...,m$, $j = 1,2,...,n$, c_1 and c_2 are positive acceleration coefficients known as the cognitive and social parameters, respectively; r_1 and r_2 are realizations of two independent random variables that assume a uniform distribution in the range [0, 1]. The best position of each particle is updated at each iteration by setting $p_i(t+1) = x_i(t+1)$, if $f_{obj}(x_i) < f_{obj}(p_i)$; otherwise, the position remains unchanged.

3.2. Optimization variables and objective function

In this study, the structure optimization design of the DOTSG, that is, pitch optimization of the inner tube of the DOTSG, is done to achieve the best combination performance for heat transfer and flow resistance. As far as the operating principle is concerned, the requirements of low pressure loss and high heat-transfer coefficient are inconsistent with one another. However, the requirement for the optimization design of the DOTSG is obtaining a shorter tube length and a lower pressure drop at the same time under specified conditions. This design problem is multi-objective optimization.

Obviously, the variable in this study is the pitch of the inner helical tube (S). However, the DOTSG is separated into three axial sections, with the sections having different thermal-−hydraulic mechanisms. As a result, the pitches in the three sections may vary. Therefore, we set the pitches in each heat-transfer section (S_{sc}, S_{bo}, S_{sh}) as three separated variables in this optimization problem. To apply the PSO method for parameter optimization of the DOTSG, the three variables are defined to compose a particle {S_{sc}, S_{bo}, S_{sh}}. Thus, there are three members in a particle.

In the optimization of the inner helical tube, minimizing the tube length is in contradiction with minimizing the pressure drop when the total heat transfer rate is given and kept constant. That is, if the target is reduction of the tube length, then the heat transfer needs to be enhanced and the pitch reduced, but these changes lead to a larger pressure drop at the same time. If the target is reduction of the pressure drop, then the pitch should be increased, but this change weakens the heat transfer in the tube, thereby increasing the tube length.
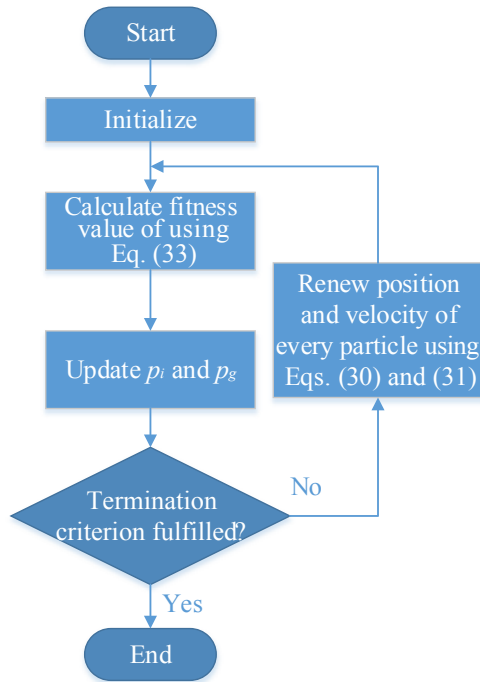
Fig. 4 − Flowchart of particle swarm optimization (PSO) for the double-tube once-through steam generator (DOTSG) optimization.

With both tube length and the pressure drop taken into consideration, the objective function is constructed through a linear weighted method, as shown in Eq. (32).

$$J = \alpha \overline{L} + \beta \overline{\Delta p} \tag{32}$$

where α and β are weight coefficients; and $\overline{L}$ and $\overline{\Delta p}$ are the normalized tube length and total pressure drop, respectively.

Considering the restrictions of manufacturing technology and the range of experimental parameters, the pitch should be in the range of 0.040 m to 0.120 m. A penalty function is needed to describe this constraint. Finally, the objective function is established in Eq. (33).

$$J = \alpha \overline{L} + \beta \overline{\Delta p} + f_p(S), \quad f_p(S) = \begin{cases} 0, & 0.040 \leq S \leq 0.120 \\ K, & S < 0.040 \ or \ S > 0.120 \end{cases} \tag{33}$$

where K is a sufficiently large constant, which is 100 here.

3.3. Application of PSO to the DOTSG optimization

For the PSO algorithm, the parameters w, c_1, and c_2, should be defined properly. The parameters c_1 and c_2 allow the particle to tune the cognition and the social terms, respectively, in the velocity update equation. Higher values of c_1 ensure a larger deviation of the particle in the search space, while higher values of c_2 signify convergence to the present global best (*gbest*) [22]. To incorporate a better compromise between the exploration and exploitation of the search space in PSO, c_1 has been allowed to decrease from the maximum value c_{max} to the minimum value c_{min}, while c_2 has been increased from c_{min} to c_{max}, as shown in Eqs. (34) and (35) [23].

$$c_1 = c_{max} - \frac{(c_{max} - c_{min})}{t_{max}} \times t \tag{34}$$

$$c_2 = c_{max} + c_{min} - c_1 \tag{35}$$

where c_{max} and c_{min} are the maximum and minimum values of acceleration coefficients, respectively; and t_{max} is the maximum iteration number.

The inertia weight w is employed to control the impact of the previous history of the velocities on the current velocity. An increase of w permits particles to explore the search space, and a decrease of w leads to a local search. Thus, to keep a balance between the local search ability and the global search ability, w is often defined as a decreasing function of time instead of a fixed constant. The parameter w starts with a large value and decreases linearly to the minimum value according to Eq. (36) [24].

$$w = w_{max} - \frac{w_{max} - w_{min}}{t_{max}} \times t \tag{36}$$

where w_{max} and w_{min} are, respectively, the maximum and minimum values of the inertia weight.

The calculation flow chart for PSO in the DOTSG optimization is shown in Fig. 4.

3.4. Results and discussion

The PSO parameters used in the present study, as well as the geometric and parametric operating conditions of the DOTSG are listed in Table 1.

On the basis of the PSO algorithm and the DOTSG model, structure optimization of the DOTSG is performed with randomly generated initial positions and velocities for the particles in the swarm. The searching process of the PSO for the DOTSG optimization is depicted in Fig. 5, and that for members of the particle during optimization is presented in Fig. 6.

Fig. 5 shows that the fitness value has been minimized to 0.42 from the initial value 0.86 in 500 iterations. Actually, the

Table 1 − Particle swarm optimization (PSO) parameters, geometric parameters, and operating conditions.

| Parameter	Value
Inner diameter of the inner helical tube (mm)	6
Outer diameter of the inner helical tube (mm)	10
Inner diameter of the outer tube (mm)	13
Outer diameter of the outer tube (mm)	18
Center distance of the outer tubes (mm)	19
Inlet pressure of the primary side (MPa)	17
Inlet pressure of the secondary side (MPa)	4
Inlet temperature of the primary side (K)	600
Inlet temperature of the secondary side (K)	379
Mass flow rate of the primary side (kg/s)	0.0179
Mass flow rate of the secondary side (kg/s)	0.0031
Swarm size	20
Maximum number of iterations	500
Maximum acceleration coefficient	2.5
Minimum acceleration coefficient	1.5
Maximum inertia weight	0.9
Minimum inertia weight	0.4
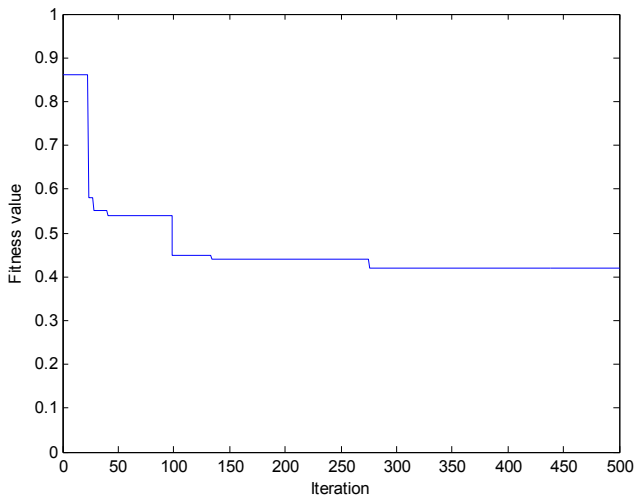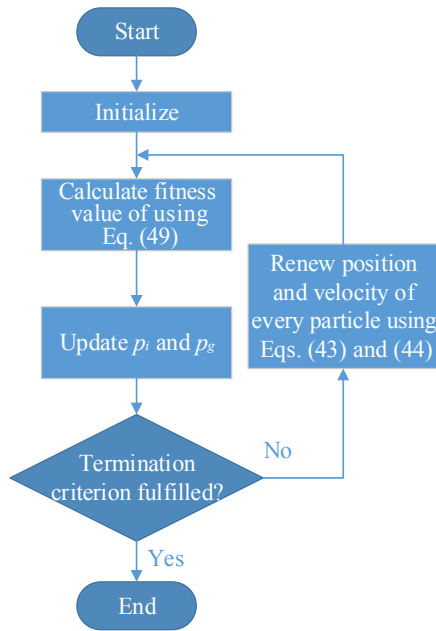
Fig. 5 – The searching process of the particle swarm optimization (PSO) for the double-tube once-through steam generator (DOTSG) optimization.

pressure drop as compared with that at S = 0.120 m. Optimized pitches can also reduce the pressure drop by 4227 Pa and increase the tube length by 0.06 m as compared with that of
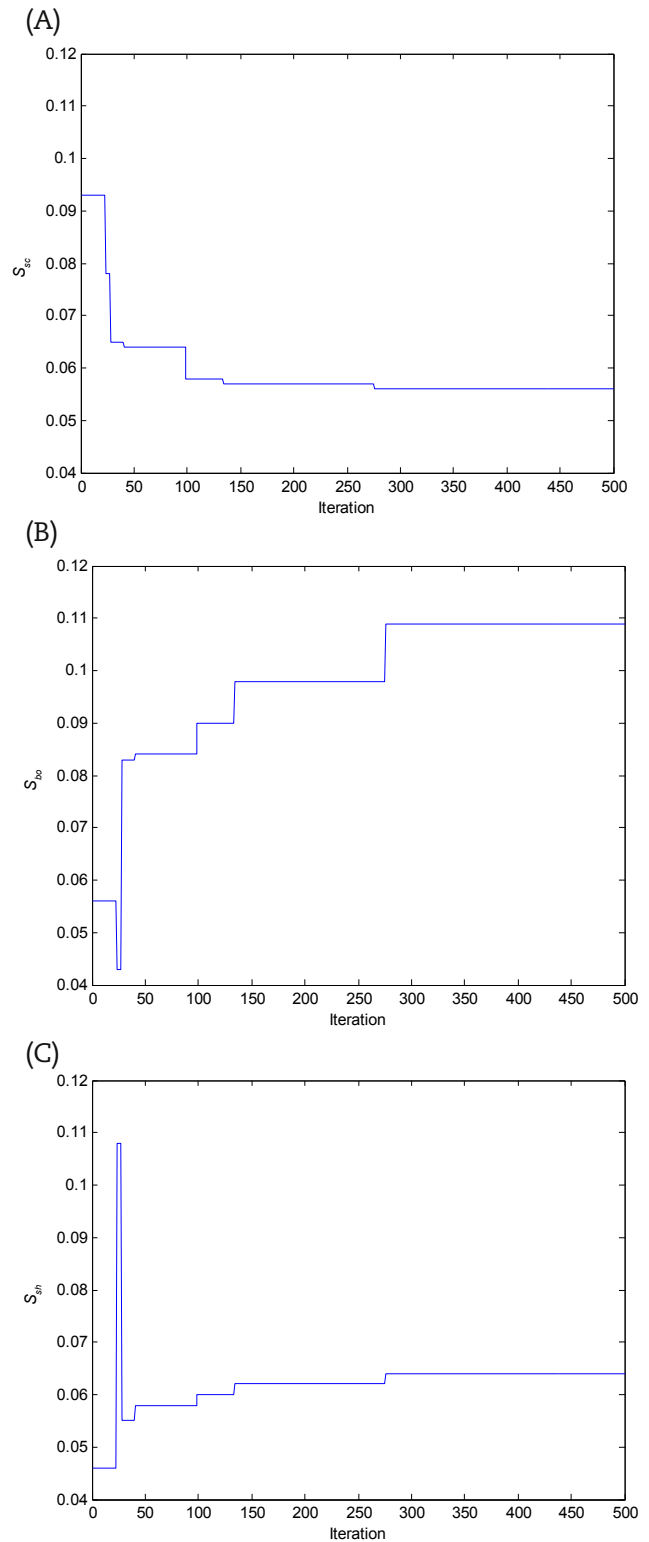

optimization was completed at the 276th step. According to Fig. 6, the best values for the three decision variables are as follows: $S_{sc} = 0.056$ m, $S_{bo} = 0.109$ m, and $S_{sh} = 0.064$ m. When the optimized pitch is obtained, the tube length and total pressure drop may be obtained as described in Section 2: $L_{op} = 0.84$ m, $\Delta p = 7642$ Pa. Therefore, the pitch distribution along the tube may be obtained from Eq. (37).

$$S_{op} = \begin{cases} 0.056 & 0 \leq L \leq 0.11 \\ 0.109 & 0.11 \leq L \leq 0.66 \\ 0.064 & 0.65 \leq L \leq 0.84 \end{cases} \qquad (37)$$

When the pitch is in its boundary values (S = 0.040 m, S = 0.120 m), L(0.040)=0.78 m, $\Delta p(0.040) = 11869$ Pa, L(0.120)= 0.87 m, $\Delta p(0.120) = 5803$ Pa, the optimized pitch can result in a 0.03-m reduction of the length and a 1439-Pa increase in the

Fig. 6 – The searching process for the members of the particle during the optimization. (A) Pitch of the subcooled section (S_{sc}); (B) pitch of the boiling section (S_{bo}); and (C) pitch of the superheated section (S_{sh}).

Table 2 – Operation parameters and structure parameters of the optimized DOTSG under 100% FP.

Operation parameters	Value	Structure parameters	Value
Primary inlet temperature (K)	600	Length of subcooled section (m)	0.18
Primary outlet temperature (K)	518	Pitch of subcooled section (m)	0.064
Secondary outlet temperature (K)	563	Length of boiling section (m)	0.54
Secondary inlet temperature (K)	379	Pitch of boiling section (m)	0.109
Primary flow rate (kg/s)	0.0179	Length of superheated section (m)	0.11
Secondary flow rate (kg/s)	0.0031	Pitch of superheated section (m)	0.056

$S = 0.040\,m$ because the inner helical tube can increase the heat transfer surface area and add to the turbulence of the fluids. These effects are strong when the pitch is small, and vice versa. We can obtain the formula for the pressure drop as Eq. (38).

$$\Delta p \, \alpha \, f \times L \qquad (38)$$

Both the increase in the fraction factor and the tube length can increase the pressure drop. Thus, the fraction factor is large and the tube length is short when the pitch is small, but the fraction factor is small and the tube length is long when the pitch is large. There must be an optimal pressure drop and a balance between the fraction factor and tube length.

As stated before, the inner helical tube can increase the heat-transfer surface area and add to the turbulence of the fluids. However, the turbulence of the mixture of water and steam during boiling is already strong; in this case, the heat transfer is enhanced by the turbulence and the effects of the inner helical tube are not needed. In addition, the strong turbulence causes a large pressure drop. Therefore, the pitch in the boiling section is larger than that in the subcooled and superheated sections at lower pressure drop and at reasonable heat-transfer rate.

4. Operation scheme design for the DOTSG

In Section 3, the optimized structure is obtained under 100% FP. However, the power level during the operation of an NPP may change, thus altering the heat duty of the DOTSG and the boundaries of the different heater-transfer sections within the fixed structure of the DOTSG. In other words, water and steam may work beyond their relevant heat-transfer sections. Operation under this condition weakens the effects of the optimization. Therefore, it is necessary to design a pertinent operation scheme for the optimized DOTSG here.

4.1. Steady-state operation analysis of the DOTSG

Under steady state, the power level of the SG equals the power level of the reactor core through heat transfer from the primary side to the secondary side, as described in Eq. (39):

$$Q = UA\Delta t_m \qquad (39)$$

where Q is the power, A is the heat-transfer area, U is the global heat transfer, and Δt_m. is the temperature difference.

For any particular SG, its heat transfer area is invariant. As indicated by Eq. (39), the steady-state power of the system can only be changed by the adjustment of U and Δt_m. Normally, the SG power level is adjusted by changing the temperature

difference and convective-heat-transfer coefficient. During the different steady-state operations, the varying pattern of the SG operating parameters may be limited by a scheduled scheme, which is known as the steady-state operation scheme [hereafter referred to as the operating scheme (OPS) for convenience]. The two typical OPSs of the NPP are the constant-primary-loop-temperature (CPT) scheme and the constant-steam-pressure (CSP) scheme. However, in many practical NPPs the OPS is the combination or modification of the two individual schemes.

The structure of the optimized DOTSG in our study cannot be changed during the power changing operation. However, the optimized pitches and boundaries of the three heat-transfer sections are designed on the basis of parameters that are under 100%, that is, at power levels below 100% FP because of mismatch of the fluid to its heat-transfer section. As a result, the pressure drop and the noise increase. Therefore, operation of the optimized DOTSG should be analyzed. First, the two traditional operation schemes are applied to the DOTSG (calculation results are discussed in this section). Optimized results in Section 3 under 100% FP are listed as calculation parameters in Table 2.

4.1.1. Constant primary-loop temperature
The CPT scheme is shown as Fig. 7. When the power level increases from 0 to 100% FP, the average temperature of the primary loop is constant, but the temperature difference
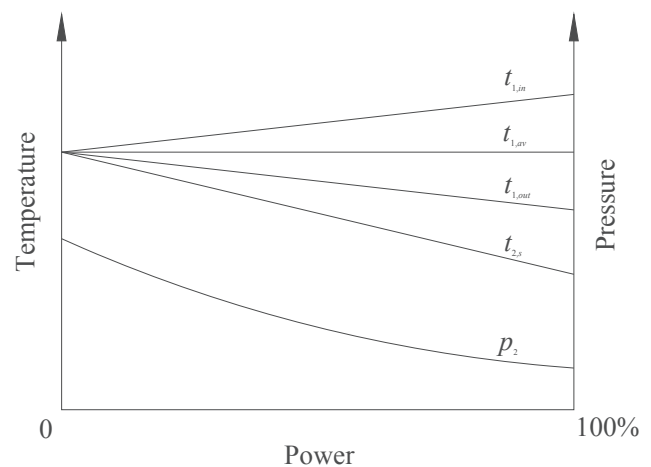

Fig. 7 – Schematic diagram of the constant-primary-loop-temperature (CPT). $t_{1,in}$ is the primary inlet temperature, $t_{1,av}$ is the primary average temperature, $t_{1,out}$ is the primary outlet temperature, $t_{2,s}$ is the secondary steam outlet temperature, p_2 is the secondary steam pressure.

Table 3 − Steady-state parameters and length of the heat-transfer sections of the double-tube once-through steam generator (DOTSG) under constant-primary-loop-temperature (CPT) from 20% to 100% full power (FP).

Po/FP	100%	90%	80%	70%	60%	50%	40%	30%	20%
$t_{1,in}$ (K)	600	596	592	588	584	580	575	571	567
$t_{1,out}$ (K)	518	522	526	530	534	538	543	547	551
$t_{2,out}$ (K)	563	573	583	585	583	578	572	567	564
$t_{1,av}$ (K)	559	559	559	559	559	559	559	559	559
G_2 (kg/s)	0.0031	0.0027	0.0024	0.0021	0.0018	0.0015	0.0012	0.0009	0.0006
L_{sc} (m)	0.18	0.16	0.14	0.12	0.10	0.09	0.08	0.06	0.05
L_{bo} (m)	0.55	0.50	0.44	0.39	0.34	0.29	0.24	0.19	0.16
L_{sh} (m)	0.11	0.18	0.26	0.33	0.40	0.46	0.52	0.59	0.63

between the hot and cold legs increases linearly. Meanwhile, the steam pressure and temperature decrease gradually.

Because the low-power condition is very different and complex, and it seldom occurs during normal operation, our calculations only deal with the operating conditions from 20% FP to 100% FP. According to the CPT, the average temperature of the primary side, the primary flow rate (G_1), and the secondary inlet temperature ($t_{2,in}$) are constant during the power level increase from 20% FP to 100% FP. Using the parameters in Table 2, we let the constant primary average temperature equal the primary average temperature under 100% FP. The other parameters can then be obtained through heat-transfer calculations under 20% to 90% FP, as shown in Table 3. Curves for the operating parameter are fitted in Fig. 8, and the boundaries of the heat-transfer sections are fitted in Fig. 9.

Table 3 and Fig. 8 show that the trends of the secondary outlet temperature and flow rate are different from those in Fig. 7. The steam temperature increases with the power level at 20% to 60% FP, reaches a peak value at approximately 60% FP, and then decreases with the power level. In Fig. 9, the boundary of the subcooled and boiling sections rises by approximately 0.1 m from 20% to 100% FP, and the boundary of the boiling and superheated sections rises by more than 0.5 m

during this process. The movement of these boundaries changes the heat-transfer areas in every section to match the power provided by the primary side and its temperature distribution. As a result, the OPS cannot be used for the operation of the DOTSG.

4.1.2. Constant steam pressure

The CSP scheme is shown in Fig. 10. Clearly, the steam pressure is constant and all of the primary temperatures increase linearly during the power level increase from 0% to 100% FP. Because the OPS is designed for the U-tube SG, which provides saturated steam, the steam temperature is also constant in Fig. 6. A constant steam temperature is used in the OPS for our study.

Similar to the calculation method in Section 4.1.1, we let the steam temperature be a constant equal to that under 100% FP by using the parameters in Table 2. The other parameters can then be obtained by heat-transfer calculations under 20% to 90% FP, as shown in Table 4. Curves for the operating parameter are fitted in Fig. 11, and the boundaries are fitted in Fig. 12.

Table 4 and Fig. 11 show that the trends of the primary side temperatures are nonlinear. Upon removal of the heat
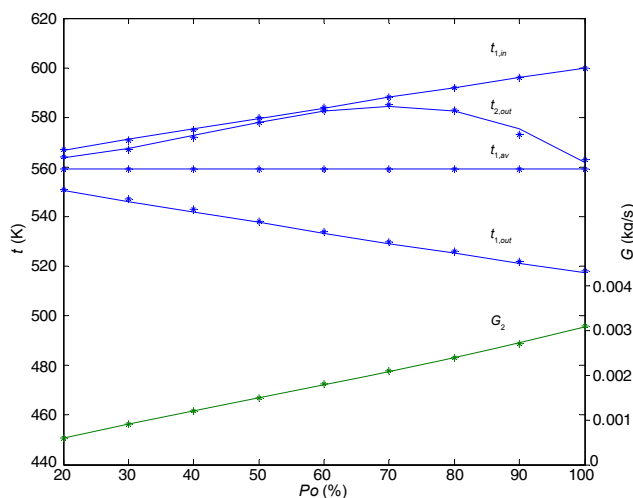

Fig. 8 − Variation of operating parameters with the power change at the constant-primary-loop-temperature (CPT). $t_{1,in}$ is the primary inlet temperature, $t_{2,out}$ is the secondary outlet temperature, $t_{1,av}$ is the primary average temperature, $t_{1,out}$ is the primary outlet temperature, G_2 is the secondary flow rate.
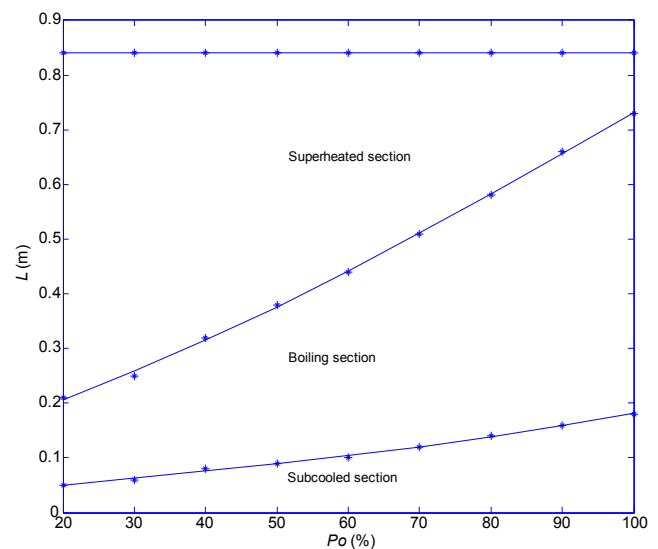

Fig. 9 − Variation of the heat-transfer boundaries of the double-tube once-through steam generator (DOTSG) at constant-primary-loop-temperature (CPT) from 20% to 100% full power (FP).
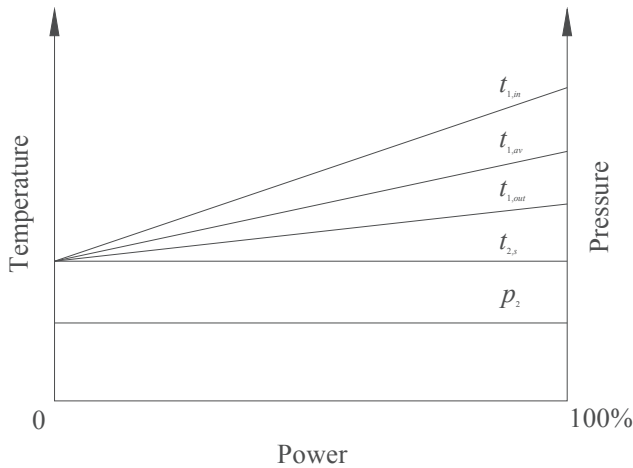
Fig. 10 − Schematic diagram of the constant-steam-pressure (CSP). $t_{1,in}$ is the primary inlet temperature, $t_{1,av}$ is the primary average temperature, $t_{1,out}$ is the primary outlet temperature, $t_{2,s}$ is the secondary steam outlet temperature, p_2 is the secondary steam pressure.

provided by the primary side, the secondary flow rate showed a linear relationship with the power level because of the difference in constant secondary temperature. In Fig. 12, the boundaries also change significantly from 20% to 100% FP; therefore, the OPS also cannot be used for the operation of the optimized DOSTG.

4.2. Fixed-boundary operation scheme

As discussed in Section 4.1, the boundaries of the heat-transfer sections change during power variation, which make the optimized structure meaningless. In other words, the real heat-transfer sections may differ from the optimized heat-transfer sections, which may lead to a higher pressure drop or ineffective heat transfer by water or steam in its inadequate section. Therefore, there is a need to design a new OPS that can provide fixed boundaries, which is defined here as the fixed-boundary (FB) scheme. According to the structure in Table 2, the lengths of every heat-transfer section and secondary inlet temperature are fixed at their reference values at 100% FP during the power increase from 20% to 100% FP. The

other parameters under 20−90% FP are calculated iteratively, as shown in Fig. 13. During this steady-state process, the temperature and the specific enthalpy can be mutually transformed according to the steam tables of The International Association for the Properties of Water and Steam (IAPWS IF-97) [25].

Step 1: An initial value for the steam temperature ($t_{2,out}$) is given.

Step 2: Calculate the secondary flow rate using Eq. (40).

$$G_2 = \frac{Q \times Po}{h_{2,out} - h_{2,in}} \tag{40}$$

Step 3: Give the primary inlet temperature ($t_{1,in}$).

Step 4: Give the outlet temperature ($t_{1,out}$).

Step 5: Calculate the primary flow rate (G_1) using Eq. (41).

$$G_1 = \frac{Q \times Po}{h_{1,in} - h_{1,out}} \tag{41}$$

Step 6: Calculate the length of the subcooled section ($L_{sc,cal}$) using Eq. (5).

Step 7: Compare $L_{sc,cal}$ with L_{sc} under 100% FP using in Eq. (42). If true, then go to Step 8; otherwise, modify $t_{1,out}$ using Eq. (43) and return to Step 5.

$$L_{sc} - L_{sc,cal} < \varepsilon \tag{42}$$

$$t_{1,out} = t_{1,out} \times \frac{L_{sc,cal}}{L_{sc}} \tag{43}$$

Step 8: Calculate the length of the boiling section ($L_{bo,cal}$) through Eq. (5).

Step 9: Compare $L_{bo,cal}$ with L_{bo} under 100% FP using Eq. (44). If true, then go to Step 10; otherwise, modify $t_{1,in}$ using Eq. (45) and return to Step 4.

$$L_{bo} - L_{bo,cal} < \varepsilon \tag{44}$$

$$t_{1,in} = t_{1,in} \times \frac{L_{bo,cal}}{L_{bo}} \tag{45}$$

Step 10: Calculate the length of the boiling section ($L_{sh,cal}$) through Eq. (5).

Step 11: Compare $L_{sh,cal}$. with L_{sh} under 100% FP using Eq. (46). If true, then save and end; otherwise, modify $t_{2,out}$ through Eq. (47) and return to Step 2.

$$L_{sh} - L_{sh,cal} < \varepsilon \tag{46}$$

Table 4 − Steady-state parameters and length of heat-transfer sections of the double-tube once-through steam generator (DOTSG) under constant-steam-pressure (CSP) from 20% to 100% full power (FP).

| Po/FP	100%	90%	80%	70%	60%	50%	40%	30%	20%
$t_{1,in}$ (K)	600	593	585	577	573	569	566	565	564
$t_{1,out}$ (K)	518	517	517	515	518	524	531	538	546
$t_{2,out}$ (K)	563	563	563	563	563	563	563	563	563
$t_{2,in}$ (K)	379	379	379	379	379	379	379	379	379
G_1 (kg/s)	0.0179	0.0179	0.0179	0.0179	0.0179	0.0179	0.0179	0.0179	0.0179
G_2 (kg/s)	0.0031	0.0028	0.0025	0.0022	0.0019	0.0016	0.0012	0.0009	0.0006
L_{sc} (m)	0.18	0.17	0.16	0.15	0.14	0.13	0.11	0.09	0.06
L_{bo} (m)	0.55	0.56	0.54	0.53	0.51	0.47	0.41	0.31	0.19
L_{sh} (m)	0.11	0.12	0.14	0.16	0.19	0.24	0.32	0.44	0.59
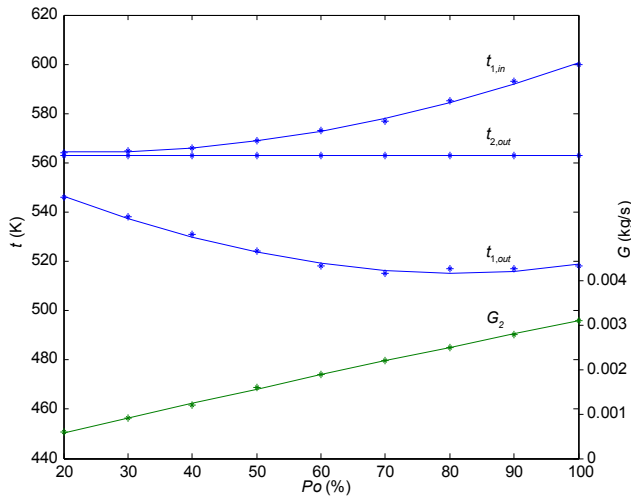
Fig. 11 − **Variation of operating parameters with the power change under constant-steam-pressure (CSP).** $t_{1,in}$ is the primary inlet temperature, $t_{2,out}$ is the secondary outlet temperature, $t_{1,out}$ is the primary outlet temperature, G_2 is the secondary flow rate.

$$t_{2,out} = t_{2,out} \times \frac{L_{sh,cal}}{L_{sh}} \qquad (47)$$

The primary inlet temperature, primary outlet temperature, secondary steam temperature, primary flow rate, and secondary flow rate under 20% to 100% FP may be obtained according to the process in Fig. 13 (Table 5).

Curves for the operating parameter are fitted with a third-order polynomial, as shown in Fig. 14 and Eqs. (48−52).
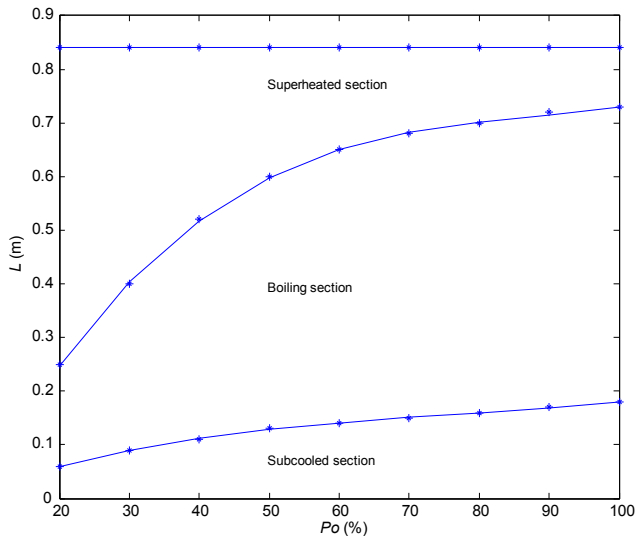
The primary inlet temperature

Fig. 12 − **Variation of the heat-transfer boundaries of the double-tube once-through steam generator (DOTSG) under constant-steam-pressure (CSP) from 20% to 100% full power (FP).**
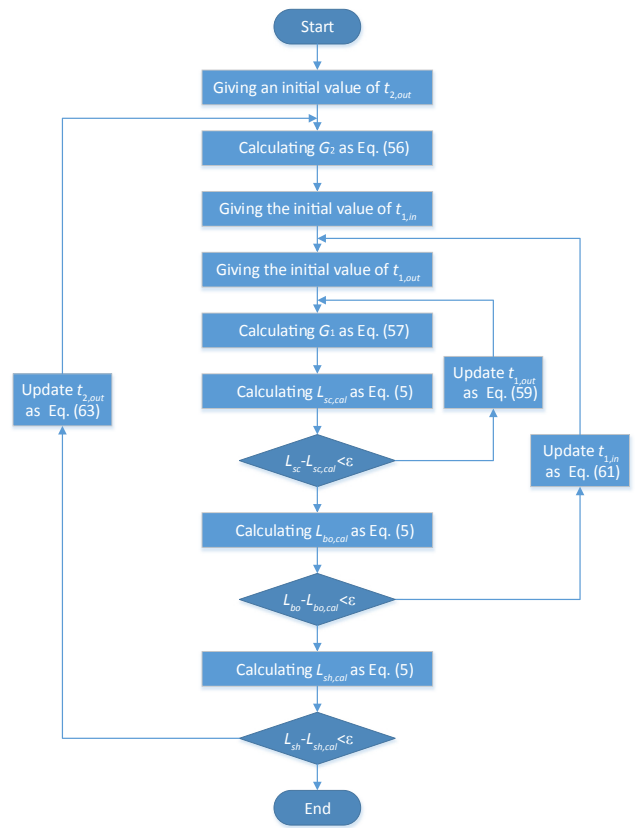

Fig. 13 − **The flow chart of the calculation of FB under a given Po. FB, fixed-boundary.**

$$t_{1,in} = -5.892Po^3 + 12.45Po^2 + 17.62Po + 576 \qquad (48)$$

The primary outlet temperature

$$t_{1,out} = 10.94Po^3 - 25.76Po^2 + 45.8Po + 486.9 \qquad (49)$$

The secondary outlet temperature

$$t_{2,out} = -21.21Po^3 + 51.19Po^2 - 41.38Po + 574.4 \qquad (50)$$

Primary flow rate
$$G_1 = -3.114 \times 10^{-3}Po^3 + 1.623 \times 10^{-3}Po^2 + 0.0197Po - 0.45 \\ \times 10^{-3} \qquad (51)$$

Feedwater flow rate

$$G_2 = -5.051 \times 10^{-4}Po^3 + 6.169 \times 10^{-4}Po^2 + 3.015 \times 10^{-3}Po - 3.57 \\ \times 10^{-5}$$

$$(52)$$

Eqs. (48−52) describe the parameters program for the FB scheme. Table 5 shows that the lengths of the three sections are constant during the power level increase from 20% to 100% FP. The optimized structure can be matched under every power level. However, the primary flow rate in the OPS needs adjustment, which is a challenge in practice. After all, this FB scheme is an exploration of the OPS design for the DOTSG, which needs more work.

Table 5 — Steady-state parameters and length of heat transfer sections of the double-tube once-through steam generator (DOTSG) under FB from 20% to 100% full power (FP).

| Po/FP	100%	90%	80%	70%	60%	50%	40%	30%	20%
$t_{1,in}$ (K)	600	598	595	592	590	587	585	582	580
$t_{1,out}$ (K)	518	515	513	510	508	504	502	499	495
$t_{2,out}$ (K)	563	563.1	563.1	563.2	563.5	563.9	564.5	566	568
$t_{2,in}$ (K)	379	379	379	379	379	379	379	379	379
G_1 (kg/s)	0.0179	0.0162	0.0148	0.0131	0.0114	0.0096	0.0073	0.0055	0.0036
G_2 (kg/s)	0.0031	0.0028	0.0025	0.0022	0.0019	0.0016	0.0012	0.0009	0.0006
L_{sc} (m)	0.18	0.18	0.18	0.18	0.18	0.18	0.18	0.18	0.18
L_{bo} (m)	0.55	0.55	0.55	0.55	0.55	0.55	0.55	0.55	0.55
L_{sh} (m)	0.11	0.11	0.11	0.11	0.11	0.11	0.11	0.11	0.11

FB, fixed-boundary.
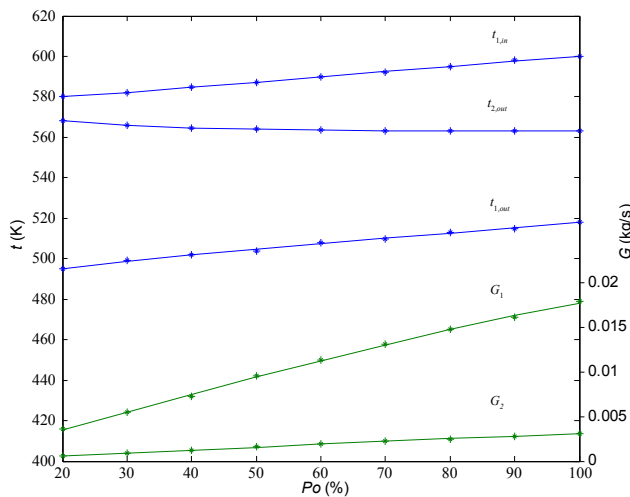
Fig. 14 — Variation of operating parameters with the power change under the FB scheme. $t_{1,in}$ is the primary inlet temperature, $t_{2,out}$ is the secondary steam outlet temperature, $t_{1,out}$ is the primary outlet temperature, G_1 is the primary flow rate. G_2 is the secondary flow rate. FB, fixed-boundary.

5.   Conclusions

The OTSG is always used in the iNPP. A DOTSG consisting of an outer straight tube and an inner helical tube is studied in this work. Such a structure can enhance the heat-transfer capacity, as well as decrease the volume and weight of the iNPP. However, the flow resistance is also increased. Therefore, the DOTSG is optimized in this study, and the OPS for the optimum DOTSG is studied.

First, the pitch of the inner helical tube is examined. The relationships of the pitch to the heat transfer and the flow resistance are analyzed. According to the different secondary fluid states, the DOTSG is axially divided into three sections: the subcooled, boiling, and superheated sections. The heat-transfer model and the flow model are established according to the different sections. The pitches in every region are selected as design variables. The combinatorial objective is composed of the tube length, the pressure drop, and a penalty function obtained through a linear weighting

method. The multi-objective optimization problem is then solved by PSO. Results for the obtained optimum pitches show that the optimum pitches are small in the single-phase sections, but large in the boiling section. The optimum pitches are 0.056 m, 0.109 m, and 0.064 m in the subcooled, boiling, and superheated sections, respectively.

To ensure the availability of the optimum structure under all power levels, a new OPS that can fix the boundaries between the subcooled, boiling, and superheated sections is proposed. The OPS is proposed on the basis of the data for the FP, and the operating parameters are calculated at low power level. The primary inlet and outlet temperatures, as well as the primary flow rate, secondary outlet temperature, and secondary flow rate are changed according to the operating procedure.

Conflicts of interest

All contributing authors declare no conflicts of interest.

Acknowledgements

REFERENCES

[1] International Atomic Energy Agency (IAEA), Advances in small modular reactor technology developments, IAEA, Austria, 2014.

[2] Z. Liu, J. Fan, Technology readiness assessment of small modular reactor (SMR) designs, Prog. Nucl. Energy 70 (2014) 20—28.

[3] S. Kang, B. Patil, J.A. Zarate, R.P. Roy, Isothermal and heated turbulent upflow in a vertical annular channel—part I. Experimental measurements, Int. J. Heat Mass Transfer 44 (2001) 1171—1184.

[4] J.A. Zarate, R.P. Roy, A. Laporta, Isothermal and heated turbulent upflow in a vertical annular channel—part II.

Numerical simulations, Int. J. Heat Mass Transfer 44 (2001) 1185—1199.

[5] Z. Wang, R. Liu, D. Jia, G. Su, S. Qiu, Heat transfer of super gas in narrow annular gap, J. Xi'an Jiaotong U. 36 (2002) 697—700.

[6] M. Chen, R. Li, B. Li, A design of compact and enhanced heat enhanced heat exchanger used in integrated nuclear reactor, 18th International Conference on Structural Mechanics in Reactor Technology, Beijing, China, 2005.

[7] J. Yu, B. Jia, Thermal hydraulic analysis of double-side heating once-through steam generator with helical tubes, Chin. J. Nucl. Sci. Eng. 26 (2006) 57—62.

[8] L.H. Costa, M. Queiroz, Design optimization of shell-and-tube heat exchangers, Appl. Therm. Eng. 28 (2008) 1798—1805.

[9] K.R. Rao, U. Shrinivasa, J. Srinivasan, Synthesis of cost optimal shell-and-tube heat exchangers, Heat Transfer Eng. 12 (3) (1991) 47—55.

[10] M. Fesanghary, E. Damangir, I. Soleimani, Design optimization of shell and tube heat exchangers using global sensitivity analysis and harmony search algorithm, Appl. Therm. Eng. 29 (2009) 1026—1031.

[11] J.M. Ponce-Ortega, M. Serna-Gonzalez, A. Jimenez-Gutierrez, Use of genetic algorithms for the optimal design of shell-and-tube heat exchangers, Appl. Therm. Eng. 29 (2009) 203—209.

[12] E. Johannessen, L. Nummedal, S. Kjelstrup, Minimizing the entropy production in heat exchange, Int. J. Heat Mass Transfer 45 (2002) 2649—2654.

[13] M.N. Ab Wahab, S. Nefti-Meziani, A. Atyabi, A comprehensive review of swarm optimization algorithms, PLoS One 10 (2015) 1—36.

[14] M. Akeari, F. Khoshahval, A. Minuchehr, A. Zolfaghari, A novel approach to find optimized neutron energy group structure in MOX thermal lattices using swarm intelligence, Nucl. Eng. Technol. 45 (2013) 951—960.

[15] W.Z. Ibrahim, Particle swarm optimization to the U-tube steam generator in the nuclear power plant, Nucl. Eng. Des. 280 (2014) 94—98.

[16] B.A. Lee, B.S. Kim, M.S. Ko, K.Y. Kim, S. Kim, Electrical resistance imaging of two-phase flow with a mesh grouping technique based on particle swarm optimization, Nucl. Eng. Technol. 46 (2014) 109—116.

[17] X. Wei, C. Dai, Y. Tai, F. Zhao, Multi-objective optimization of double-tube once-through steam generator, J. Heat Transfer 134 (2012) 071801.

[18] H. Fang, X. Wei, F. Zhao, Structural optimization of double-tube once-through steam generator using Pontryagin's maximum principle, Prog. Nucl. Energy 78 (2015) 318—329.

[19] V.M. Budov, S.M. Dmitriev, Heat transfer enhancement in narrow annuli, Two-Phase Flow Energy Mach. 3 (1985) 122—124.

[20] V.M. Budov, S.M. Dmitriev, Influence of the helical flow on the bilaterally heated channels, Issues At. Sci. Technol. 6 (1987) 72—76.

[21] Z.L. Gaing, A particle swarm optimization approach for optimum design of PID controller in AVR system, IEEE Trans. Energy Appar. Syst. 19 (2004) 384—391.

[22] P.K. Tripathi, S. Bandyopadhyay, S.K. Pal, Multi-objective particle swarm optimization with time variant inertia and acceleration coefficients, Inf. Sci. 177 (2007) 5033—5049.

[23] R. Coban, Power level control of the TRIGA mark-II research reactor using the multi feedback layer neural network and the particle swarm optimization, Ann. Nucl. Energy 69 (2014) 260—266.

[24] O. Safarzadeh, A. Zolfaghari, M. Zangian, O. Noori-kalkhoran, Pattern optimization of PWR reactor using hybrid parallel artificial bee colony, Ann. Nucl. Energy 63 (2014) 295—301.

[25] W. Wagner, J.R. Cooper, A. Dittmann, J. Kijima, H.J. Kretzschmar, A. Kruse, R. Mareš, K. Oguchi, H. Sato, Y. Takaishi, I. Tanishita, J. Trübenbach, T. Willkommen, The IAPWS industrial formulation 1997 for the thermodynamic properties of water and steam, J. Eng. Gas Turbines Power 122 (2000) 150—182.